利用二维反射镜实现无线光通信快速对准

杨尚君[1]，柯熙政[1,2,3*]，吴加丽[1]，刘旭光[4]

[1]西安理工大学自动化与信息工程学院，陕西 西安 710048；

[2]陕西省智能协同网络军民共建重点实验室，陕西 西安 710048；

[3]陕西理工大学物理与电信工程学院，陕西 汉中 723001；

[4]西安理工大学自动化与信息工程学院通信工程系，陕西 西安 710048

摘要 针对无线光通信存在光束对准耗时长的问题，提出一种发射端采用图像跟踪，接收端采用二维反射镜控制的光束快速对准方法。依据几何光学理论计算了激光经二维反射镜后出射的扫描轨迹，并在无线光通信强度调制/直接检测系统上开展实验。实验结果表明：当通信距离为 1.3 km 时，光斑型心在 $x(y)$ 方向的方差由跟踪前的 12.5734 $pixel^2$（5.1393 $pixel^2$）降至跟踪后的 2.2770 $pixel^2$（1.3697 $pixel^2$），探测器输出电信号的幅值为 92.4 mV；当通信距离为 10.3 km 时，光斑型心在 $x(y)$ 方向的方差由跟踪前的 18.8653 $pixel^2$（10.5290 $pixel^2$）降至跟踪后的 14.4970 $pixel^2$（8.0287 $pixel^2$），探测器输出电信号的幅值为 74.4 mV。所提方法无需将控制信号由接收端回传至发射端，在快速建立下行链路的同时即可实现上行链路的建立。

关键词 光通信；光束扫描；捕获跟踪对准；二维反射镜

中图分类号 TN929.1　　　　**文献标志码** A　　　　　　　　　　　　**DOI**：10.3788/CJL202249.1106001

1 引　　言

无线光通信具有速率高、保密性好和抗干扰能力强等优点，逐渐成为海量数据传输的最优通信手段之一[1]。建立无线光通信的前提是通信双方光端机的收发视轴保持精确对准和实时跟踪[2-4]。由于激光具有光束窄、方向性强等特点，信号光束需要极其精确的指向[5-6]。激光信号在大气信道中传输时，由大气湍流引起的大气折射率起伏导致传输过程中出现光束扩展、光束漂移、波前畸变等现象，对光信号的接收造成了不利的影响，严重时甚至会导致通信中断[7-8]。在无线光通信系统中，一般采用凝视-凝视、凝视-扫描、跳步-扫描这 3 种捕获方法来实现发射天线与接收天线的光束同轴对准[9]，这就增加了系统通信的准备时间。实际中需要一种快速的捕获、跟踪与对准（ATP）机制来建立链路[10-12]。

采用复合轴的 ATP 系统以矩形或者螺旋形进行光束扫描[13]，接收端通过卫星定位系统进行数据解算[14]，并利用成像装置进行图像采集[15]，最终实现光束的捕获。利用大视场、窄带宽的粗跟踪和小范围、宽带宽的精跟踪相结合的方式，粗跟踪使信标光斑进入精跟踪视场[16]，精跟踪对粗跟踪残差进行进一步抑制[17]。位置敏感传感器、四象限探测器[18-19]、电荷耦合器件[20-22]等是常用的位置反馈器件。Bao 等[23]提出一种基于图像传感器像素响应光斑尺度面积的平场模型及校正方法；Zhang 等[24]将分段低阶多项式最小二乘拟合和卡尔曼滤波器相结合，提出一种采用四象限探测器进行点位置检测的方法；陈刚等[25]采用位置敏感探测器实现对激光通信系统的光束跟踪与控制；Tolker-Nielsen 等[26]采用光束粗检测与精检测分离的双电荷耦合器件检测方案，设计出无线光卫星通信系统终端的 ATP 系统。

二维反射镜作为跟踪系统中的执行机构,最初被用于自适应光学系统波前倾斜畸变的补偿[27],随后被用于光束扫描、光束定位、目标跟踪等领域。由压电陶瓷驱动的二维反射镜具有扫描角度小、谐振频率高的特点,但也存在补偿迟滞和蠕变的固有缺陷[28-29]。左韬等[30]基于压电二维反射镜采用自校正控制在 2.3 km 范围内实现了光束的精跟踪;Jono 等[31]针对激光通信设备的 APT 系统,采用粗跟踪与精跟踪嵌套的复合轴控制技术,粗跟踪系统采用二维转台结构,精跟踪系统由压电二维反射镜构成;Borrello 等[32]采用位置敏感传感器和压电二维反射镜,实现了发射激光器到光检测器之间50 km 精确的稳定视线对准,完成了宽视场角下的跟踪;Suite 等[33]在无线光通信的接收器上安装了由位置敏感传感器控制的二维反射镜激光通信测试设备,实现了光束的跟踪。由音圈电机驱动的二维反射镜具有扫描角度大、谐振频率高的特点。王福超等[34]采用完全跟踪控制方法,拓展了由音圈电机驱动的快速反射镜的控制带宽;Wu 等[35]设计了一

种具有高密度线通量结构的音圈电机二维反射镜,从而降低了反射镜的漏磁性及受干扰特性;陈国真等[36]采用柔性解耦机构来消除电机动子的横向位移,设计了变值陷波滤波器来消除随位置变化的共振模态的影响。

本文针对传统 ATP 系统存在对准耗时长的缺点,提出一种光束快速对准的方法。该方法在发射端采用图像标定,在接收端采用二维反射镜控制,通过改变二维反射镜的俯仰角和方位角实现光束扫描,以焦平面光斑的位置信息反馈实现光束跟踪,并在无线光通信强度调制/直接检测(IM/DD)系统的基础上分别进行了 1.3 km 和 10.3 km的外场实验。

2 理论计算

无线光通信系统同轴对准方式如图 1(a)所示,要求发射天线的光轴和接收天线的光轴在空间上完全重合。大气湍流引起光束漂移,需要通过探测器回传测量数据,以调整发射天线,使光束
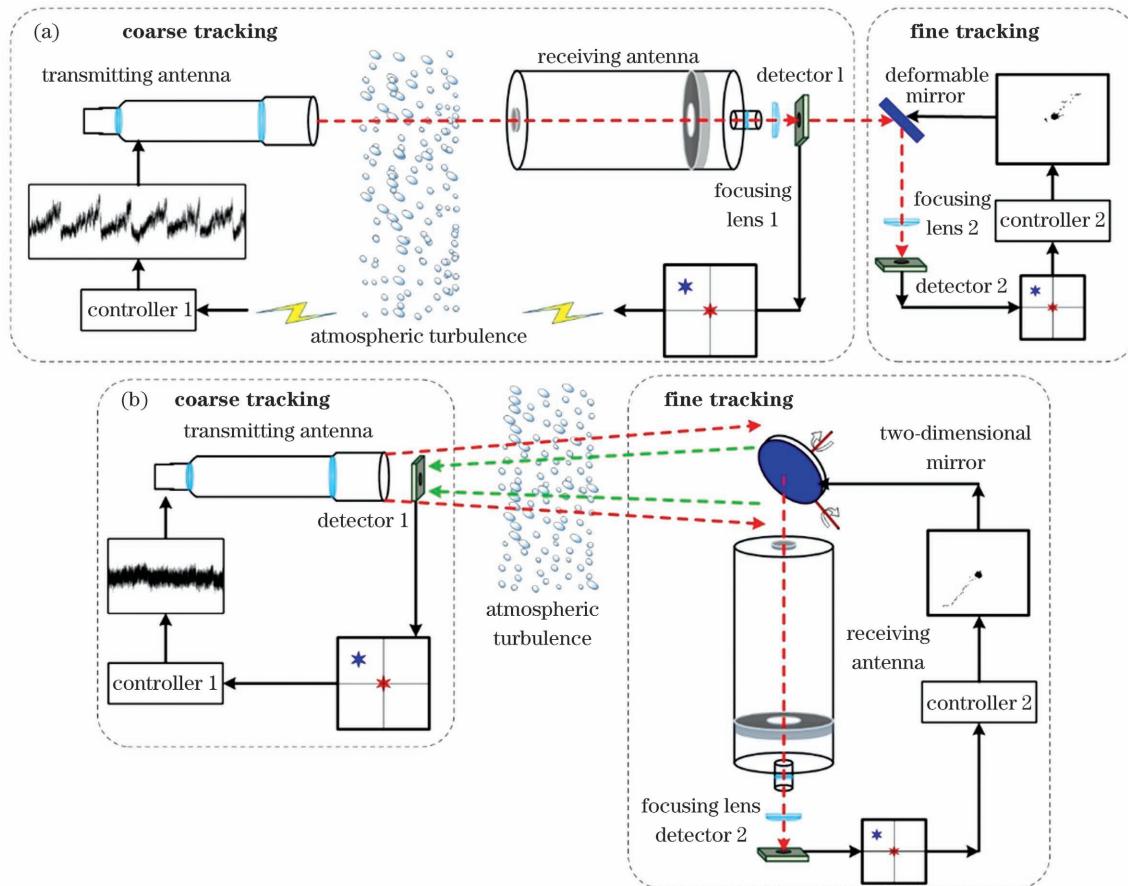

图 1 无线光通信光束对准示意图。(a)同轴对准;(b)二维反射镜辅助对准
Fig. 1 Schematic of beam alignment of wireless optical communication. (a) Coaxial alignment; (b) two-dimensional mirror assisted alignment

保持长时间稳定的粗对准,以及在此基础上的精对准。远距离数据回传和位置调整受大气湍流影响,导致传统的长轴光束对准过程中不确定因素较多。

图 1(b)所示为采用二维反射镜辅助对准的无线光通信系统,该系统由发射天线到二维反射镜的标定粗对准系统和二维反射镜到接收天线的短轴精对准系统组成。在从发射天线到二维反射镜的标定粗对准系统中,采用发射端的标定相机直接进行定位标定,以图像为反馈调整发射天线;在从二维反射镜到接收天线的短轴精对准中,根据接收天线后端的探测器反馈信息调节二维反射镜。由于标定粗对准和短轴精对准均在单端即可操作,发射端标定对准无需回传数据,该对准方式便捷且受环境的影响较小。

为了研究光线经二维反射镜后在出射面的扫描轨迹,建立如图2所示的空间坐标系[37]。入射
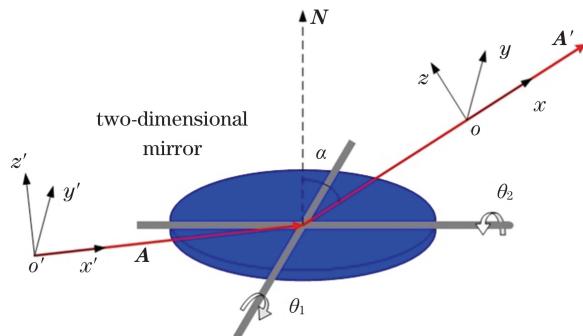
图 2 二维反射镜的几何光学模型

Fig. 2 Geometrical optical model of two-dimensional mirror

光线的矢量记为 A,出射光线与二维反射镜面法线的夹角为 α,以入射光线的矢量方向为 x' 轴,建立入射光线的空间坐标系 o'-$x'y'z'$。出射光线的矢量记为 A'。以出射光线的矢量方向为 z 轴,建立出射光线的空间坐标系 o-xyz。镜面的法向量为 N,二维反射镜的在横、纵轴方向的偏转角分别为 θ_1、θ_2。

以 o-xyz 坐标系为主坐标系,A 和 N 的矢量表达式分别为

$$A = \begin{bmatrix} A_x \\ A_y \\ A_z \end{bmatrix} = \begin{bmatrix} -\sin(2\alpha) \\ 0 \\ -\cos(2\alpha) \end{bmatrix}, \tag{1}$$

$$N = \begin{bmatrix} N_x \\ N_y \\ N_z \end{bmatrix} = \begin{bmatrix} \sin(\alpha + \theta_1) \cdot \cos\theta_2 \\ \sin\theta_2 \\ \cos(\alpha + \theta_1) \cdot \cos\theta_2 \end{bmatrix}. \tag{2}$$

由反射定律可知,A、A' 和 N 的夹角相等,因此反射定律的矢量表达式为

$$A' = A - 2(A \cdot N) \cdot N = MA, \tag{3}$$

$$N(\theta) = N \cdot \cos\theta + C(C \cdot N) \cdot (1 - \cos\theta) + (C \times N) \cdot \sin\theta, \tag{4}$$

式中:C 为任一旋转轴方向对应的单位方向向量。将式(1)、式(2)、式(4)代入式(3),得到矩阵 M:

$$M = \begin{bmatrix} 1 - 2N_x^2 & -2N_xN_y & -2N_xN_z \\ -2N_xN_y & 1 - 2N_y^2 & -2N_yN_z \\ -2N_xN_z & -2N_yN_z & 1 - 2N_z^2 \end{bmatrix}. \tag{5}$$

将式(1)、式(2)代入式(5),可得出射光线的矩阵形式:

$$A' = \begin{bmatrix} A'_x \\ A'_y \\ A'_z \end{bmatrix} = \begin{bmatrix} \sin(2\alpha) \cdot [2\cos^2\theta_2 \cdot \sin^2(\alpha + \theta_1) - 1] + \cos(2\alpha) \cdot \cos^2\theta_2 \cdot \sin(2\alpha + 2\theta_1) \\ \cos(2\alpha) \cdot \cos(\alpha + \theta_1) \cdot \sin(2\theta_2) + \sin(2\alpha) \cdot \sin(\alpha + \theta_1) \cdot \sin(2\theta_2) \\ \cos(2\alpha) \cdot [2\cos^2\theta_2 \cdot \cos^2(\alpha + \theta_1) - 1] + \sin(2\alpha) \cdot \cos^2\theta_2 \cdot \sin(2\alpha + 2\theta_1) \end{bmatrix}. \tag{6}$$

扫描光斑在 xoy 平面的坐标为

$$x = L\frac{A'_x}{A'_z} = L\frac{\sin(2\alpha) \cdot [2\cos^2\theta_2 \cdot \sin^2(\alpha + \theta_1) - 1] + \cos(2\alpha) \cdot \cos^2\theta_2 \cdot \sin(2\alpha + 2\theta_1)}{\cos(2\alpha) \cdot [2\cos^2\theta_2 \cdot \cos^2(\alpha + \theta_1) - 1] + \sin(2\alpha) \cdot \cos^2\theta_2 \cdot \sin(2\alpha + 2\theta_1)}, \tag{7}$$

$$y = L\frac{A'_y}{A'_z} = L\frac{\cos(2\alpha) \cdot \cos(\alpha + \theta_1) \cdot \sin(2\theta_2) + \sin(2\alpha) \cdot \sin(\alpha + \theta_1) \cdot \sin(2\theta_2)}{\cos(2\alpha) \cdot [2\cos^2\theta_2 \cdot \cos^2(\alpha + \theta_1) - 1] + \sin(2\alpha) \cdot \cos^2\theta_2 \cdot \sin(2\alpha + 2\theta_1)}, \tag{8}$$

式中:L 为从光束反射点到 xoy 平面的距离。

图 3 为采用二维反射镜的激光跟踪算法示意图,利用红外相机获取光斑的位置信息,并将位置信息通过计算转化为二维反射镜的调整角度值,通过调节二维反射镜,实现光束的跟踪和控制。记探测器中心点的探测位置为 (m_c, n_c),红外相机成像光斑的位置为 $(m(k), n(k))$,则第 $k+1$ 次施加在二维反射镜的俯仰角 θ_1 和方位角 θ_2 的指令为

$$\begin{bmatrix} \theta_1(k+1) \\ \theta_2(k+1) \end{bmatrix} = \begin{bmatrix} m(k) - m_c \\ n(k) - n_c \end{bmatrix} \cdot T \cdot K_i + \begin{bmatrix} \theta_1(k) \\ \theta_2(k) \end{bmatrix}, \tag{9}$$
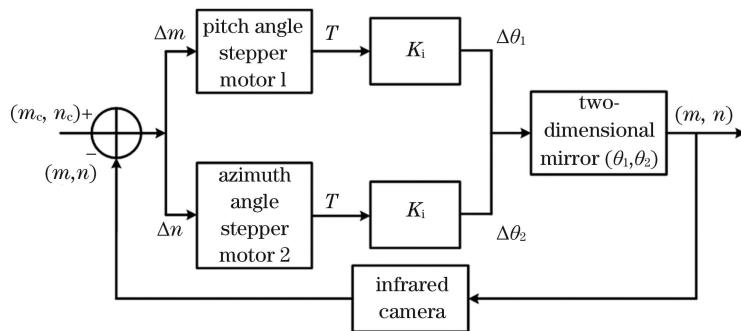
图 3　采用二维反射镜的激光跟踪算法示意图

Fig. 3　Laser tracking algorithm block diagram using two-dimensional mirror

式中：T 为由电机角度转化为像素位移的单位转化系数；K_i 为积分常数。

完成光束跟踪后，含有信源信息的强度调制光信号经过聚焦透镜耦合进入光电探测器，强度调制器的半波电压为 V，调整强度调制器的直流偏置电压 V_{bias} 实现光信号强度调制和直接探测。

$$V_{out}(t) = \left\langle \eta \cdot \int_s \left[E_{in} \cos \left\{ \frac{\pi}{2V_\pi} [V_m(t) - V_{bias}] \right\} \exp \left(j \frac{\pi V_{bias}}{2V_\pi} \right) \right]^2 ds \right\rangle R, \quad (10)$$

式中：$V_{out}(t)$ 为探测器输出电压信号；$V_m(t)$ 为加载到调制器的信源信号；$E_{in}(t)$ 为调制器输入光信号；s 为探测器有效面积；h 为探测器响应度；R 为输出阻抗。

3　实验研究

3.1　系统组成

基于以上理论研究，搭建了图 4 所示的利用二维反射镜实现快速对准的无线光通信 IM/DD 系统。发射端采用强度外调制的方式将信源加载到光波上，经光纤放大器由发射天线进行准直发射输出。利用位于发射端的瞄准平台和标定相机对接收端的二维反射镜完成初始标定，使光束完全覆盖到接收端的二维反射镜面上，调节二维反射镜使反射光束与接收天线共轴对准。由接收天线出射的平行光经过分光棱镜分为两束，一路经聚焦透镜会聚后，耦合进入光电探测器感光面，用于系统通信；另一路光束经聚焦后，利用红外相机对光斑位置进行实时检测，完成光束的跟踪。表 1 为主要的实验设备以及对应的参数。

3.2　1.3 km 外场实验

图 5 为基于 IM/DD 的无线光通信快速对准 1.3 km 外场实验示意图，发射端和接收端分别为西安市南二环凯森福景雅苑和西安理工大学教六楼。测量时间为 2021 年 4 月 16 日，天气晴，西南风 2 级，大气相干长度 r_0 为 26.3 cm，大气湍流格林伍德频率为 0.83 Hz。
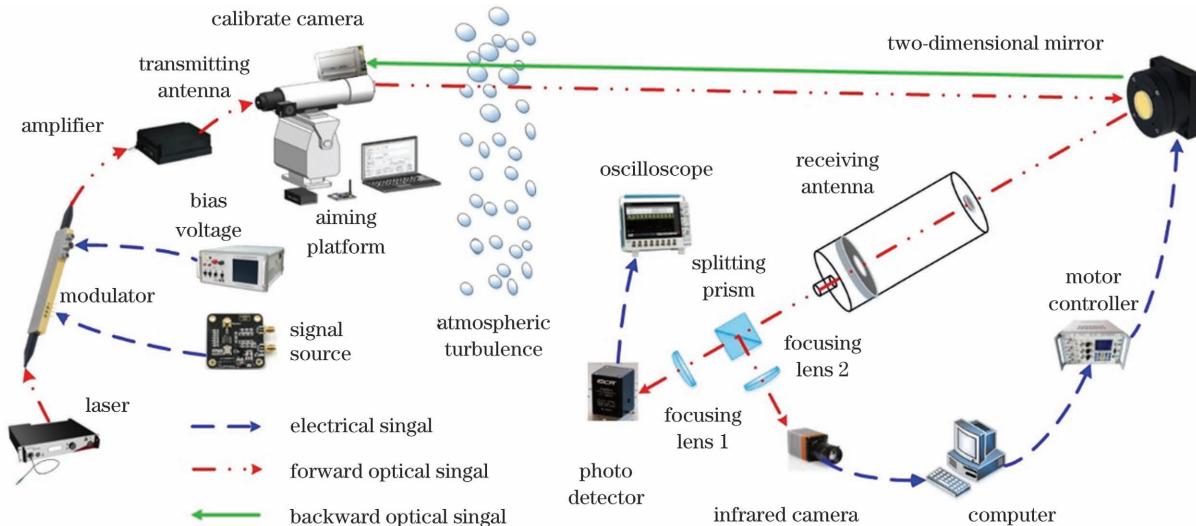

图 4　采用二维反射镜快速对准的 IM/DD 的无线光通信系统

Fig. 4　Wireless optical communication IM/DD system with fast alignment of two-dimensional mirror

表 1 实验设备及参数

Table 1 Experimental equipment and parameters

| Experimental equipment	Main parameter
Modulator	X-cut crystal Radio frequency drive voltage：$V_m = 4.5$ V Half-wave voltage：$V_p = 5.5$ V
Antenna	Transmitting antenna：Cassegrain with diameter of 105 mm Receiving antenna：Cassegrain with diameter of 220 mm
Calibrate camera	Digital zoom Up to 128×7.5 mm Pixel resolution：640 pixel$\times$480 pixel Pixel size：1 pixel$=20$ μm
Two-dimensional mirror	Diameter：280 mm Resonant frequency：20 Hz Resolution：2.73 μrad
Infrared camera	Detector type：InGaAs Wavelength range：0.9–1.7 μm Pixel resolution：320 pixel$\times$256 pixel Pixel size：1 pixel$=20$ μm
Photo detector	Detector type：InGaAs Cut-off frequency：30 kHz–1.5 GHz Effective area diameter：100 μm
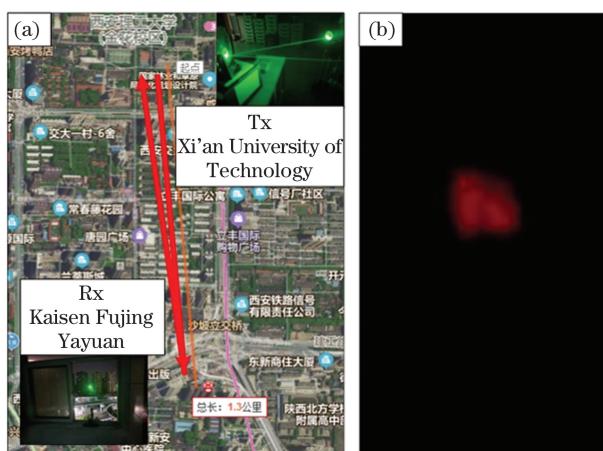
图 5 无线光通信系统 1.3 km 外场实验示意图。(a)链路图；(b)远场光斑

Fig. 5 Schematic of field experiment of wireless optical communication for 1.3 km. (a) Link diagram；(b) far field spot

图 6(a)为采用标定相机进行快速标定和跟踪的结构示意图。先将发射端的标定相机和发射天线装调成平行共轴光学系统，通过调节伺服电机的俯仰角和方位角，以及标定相机的变焦系统，逐步寻找位于接收端的二维反射镜的参考坐标位置，当相机中心与二维反射镜的参考坐标位置（当标定相机的极限观测距离不足时，可选用近点共轴参照系）重合时，根据光路可逆原理，即认为光束完成了长轴粗对准。图 6(b)所示为经调整后标定相机的成像位置中心与接收端参考坐标位置重合的上位机界面。

光束粗对准后，以标定点和二维反射镜成像坐标位置的相对偏差进行光束粗跟踪，图 7 所示为 1.3 km 实验链路下二维反射镜位置坐标的光束粗跟踪曲线，其中俯仰角在 4 h 内调整了 2 次，方位角在 4 h 内调整了 1 次，受到由大气湍流引起的光束漂移和光机结构自身重力的影响，粗对准在短时间内无需频繁调整。


图 6 光束快速标定示意图。(a)结构图；(b)标定相机界面

Fig. 6 Schematic of beam fast calibration. (a) Structure diagram；(b) calibration camera interface
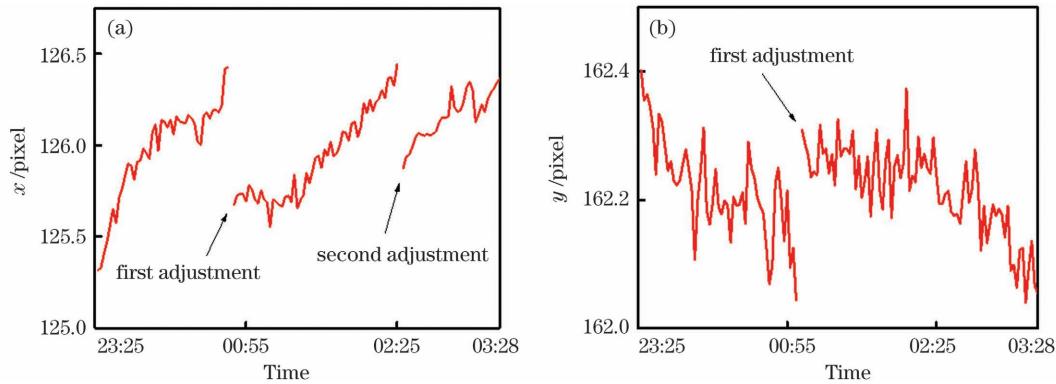
图 7 不同调整情况下标定相机系统 1.3 km 外场实验的跟踪曲线。(a)俯仰调整;(b)方位调整

Fig. 7 Tracking curves of calibration camera system in 1.3 km field experiment under different adjustments. (a) Pitch adjustment; (b) azimuth adjustment

依据式(7),设标定后二维反射镜中心到探测器表面的距离 L 为单位 1,分别对经不同入射角 α、不同扫描角度 θ_1、θ_2 调整后光束在接收面描绘出的轨迹进行计算。图 8 所示为不同参数下反射光束的扫描轨迹,扫描轨迹曲线呈现出以弧形为基础形状的截面图,入射角度 α 决定了扫描轨迹的弧度,扫描角度 θ_1、θ_2 决定了扫描平面的扫描面积。根据入射角度 α 和二维反射镜中心到探测器表面的距离 L,选择合适的扫描角度范围以及扫描步距,可在短时间内实现光斑快速捕获。
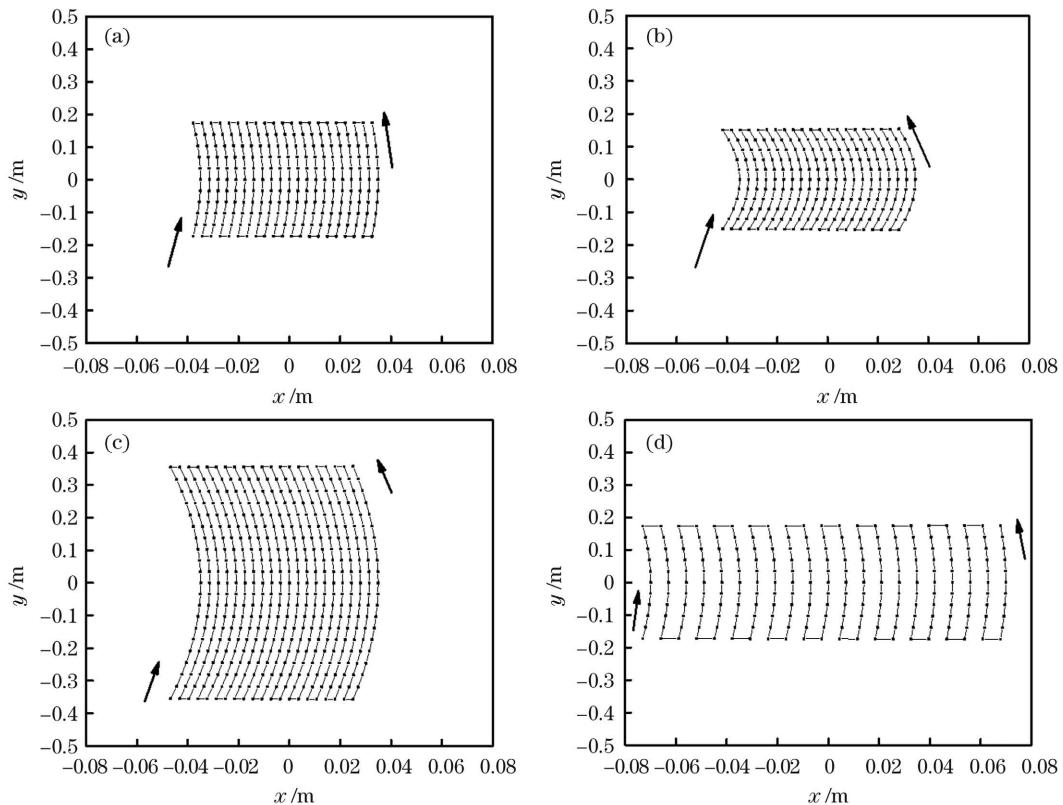
图 8 不同入射角度和扫描角度下出射光斑轨迹图。(a)$\alpha=10°$,$\theta_1=-1°\sim1°$,$\theta_2=-5°\sim5°$;(b)$\alpha=30°$,$\theta_1=-1°\sim1°$,$\theta_2=-5°\sim5°$;(c)$\alpha=10°$,$\theta_1=-1°\sim1°$,$\theta_2=-10°\sim10°$;(d)$\alpha=10°$,$\theta_1=-2°\sim2°$,$\theta_2=-5°\sim5°$

Fig. 8 Trajectories of outgoing spot under different incident angles and scanning angles. (a) $\alpha=10°$, $\theta_1=-1°-1°$, $\theta_2=-5°-5°$; (b) $\alpha=30°$, $\theta_1=-1°-1°$, $\theta_2=-5°-5°$; (c) $\alpha=10°$, $\theta_1=-1°-1°$, $\theta_2=-10°-10°$; (d) $\alpha=10°$, $\theta_1=-2°-2°$, $\theta_2=-5°-5°$

当光斑位于红外相机中心位置时,分别计算 x 方向和 y 方向光斑型心变化的均值方差和功率谱密度(PSD),其中 x 方向光斑型心漂移均值为 161.7439 pixel,方差为 12.5734 $pixel^2$,y 方向光斑

型 心 漂 移 均 值 为 121.3437 pixel，方 差 为 18.8653 pixel²。图 9 所示为光斑型心在 x 方向和

y 方向漂移的功率谱密度，功率谱分量以低频成分为主，说明此时光斑型心漂移缓慢。
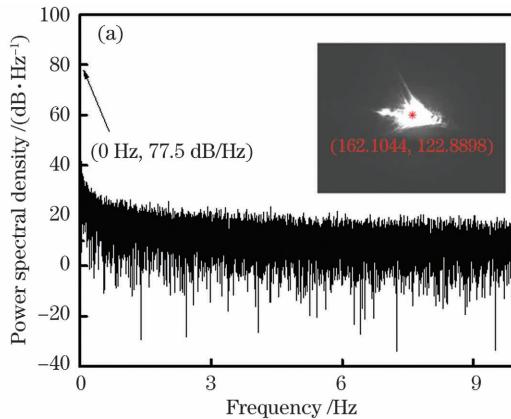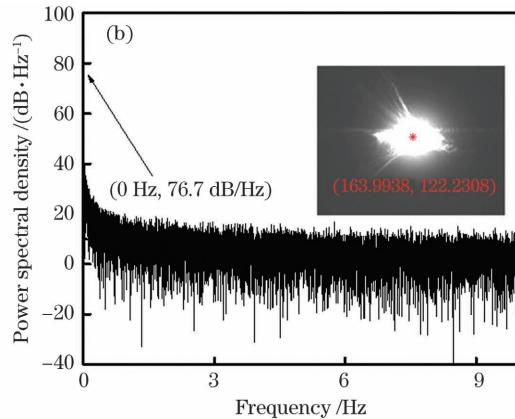
图 9　1.3 km 外场实验中光斑型心漂移量功率谱密度。(a)x 方向；(b)y 方向

Fig. 9　Power spectral density of spot center drift in 1.3 km field experiment. (a) x direction; (b) y direction

图 10 所示为 1.3 km 外场实验中光束跟踪轨迹以及对应的时域波形和功率谱密度估计，二维反射镜调整步进角为 10.92 μrad，依据式（9），随着迭代次数的增加，光斑的型心从探测面的第一象限逐

步调整至中心位置。经跟踪发现，位于相机中心的光斑型心在 x 方向和 y 方向的方差分别为 2.2770 pixel² 和 1.3697 pixel²，系统完成一次闭环所需的时间为 0.05 s，足以补偿光斑的漂移速率。

图 10　1.3 km 外场实验的跟踪波形。(a)跟踪轨迹；(b)x、y 方向跟踪曲线；(c)x 方向功率谱密度；(d)y 方向功率谱密度
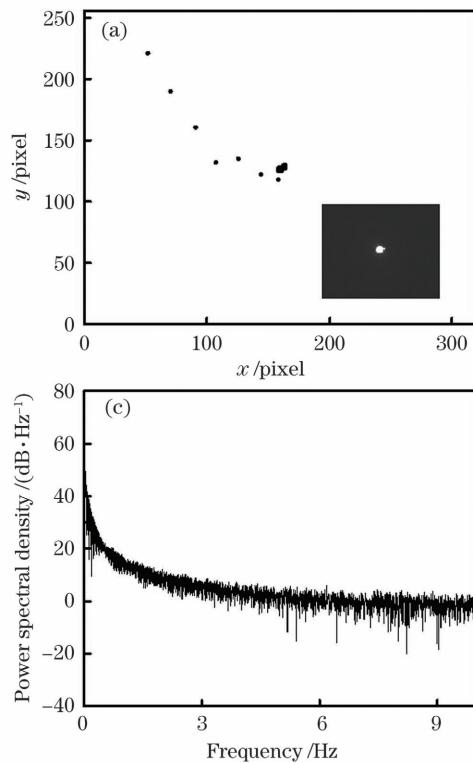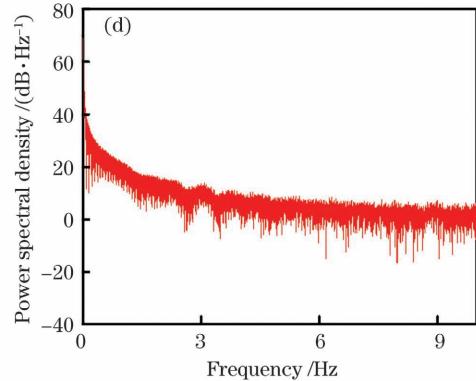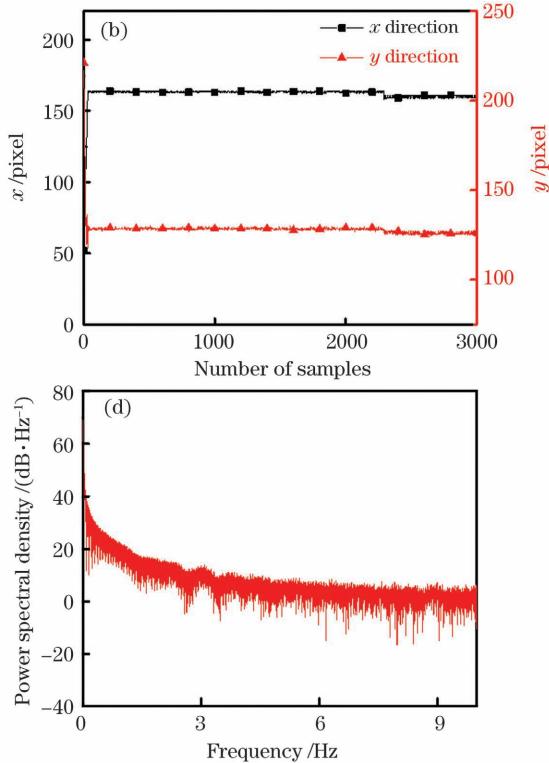
Fig. 10　Tracking waveforms in 1.3 km field experiment. (a) Tracking curve; (b) track curves along x and y directions; (c) power spectral density along x direction; (d) power spectral density along y direction

当光束完成跟踪后，位于探测器支路的光束经聚焦透镜耦合进入探测器感光面内，图 11(b)所示为经跟踪处理后探测器的输出波形，当发射功率为 15 mW 时，探测器输出波形的幅值为 92.4 mV。

3.3　10.3 km 外场实验

在 1.3 km 外场实验的基础上，开展了快速对准的 10.3 km 外场实验，图 12(a)为 10.3 km 实验链路图，发射端和接收端分别位于西安市白鹿原肖
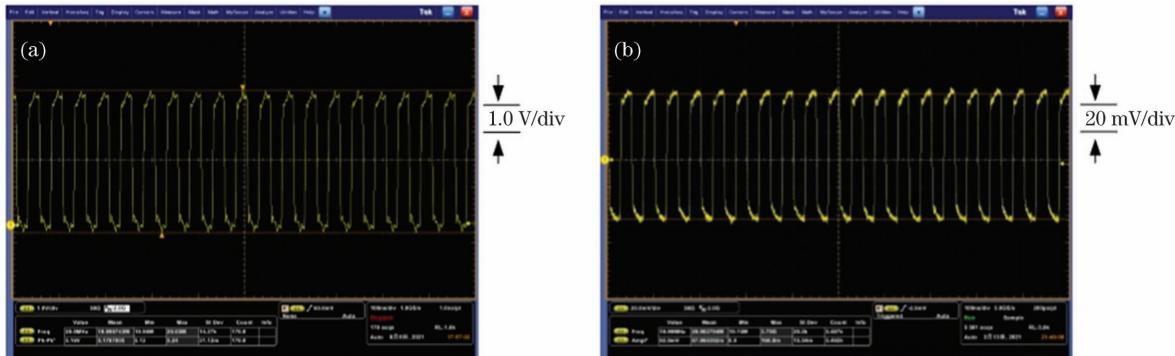
图 11 通信链路 1.3 km 信号波形。(a)发射信号;(b)接收信号

Fig. 11 Signal waveforms at 1.3 km communication link. (a) Transmitting signal; (b) receiving signal
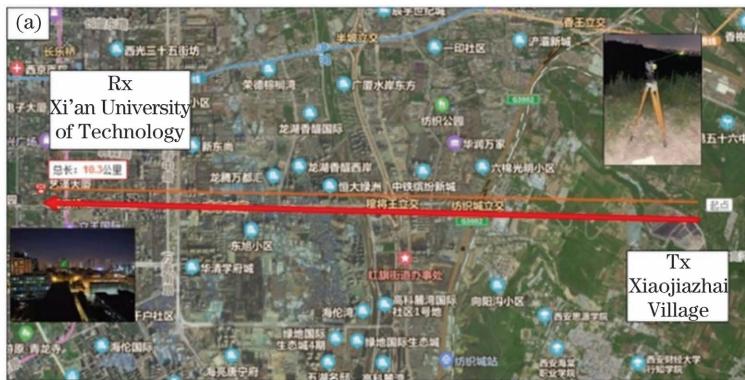
图 12 无线光通信系统 10.3 km 外场实验示意图。(a)链路图;(b)远场光斑

Fig. 12 Schematic of wireless optical communication system in 10.3 km field experiment. (a) Link diagram; (b) far field spot

家寨村和西安理工大学教六楼。测量时间为 2021 年 7 月 24 日,天气晴,东风 2 级,大气相干长度 r_0 为 10.8 cm,大气湍流格林伍德频率为 12.71 Hz。

图 13 所示为 10.3 km 链路下经粗对准后的二维反射镜成像位置的坐标跟踪曲线,其中在 6 h 内,俯仰角进行了 4 次调整,方位角进行了 2 次调整,由强湍流引起的光束漂移使得 10.3 km 下光束漂移范围的粗跟踪频率均高于 1.3 km。
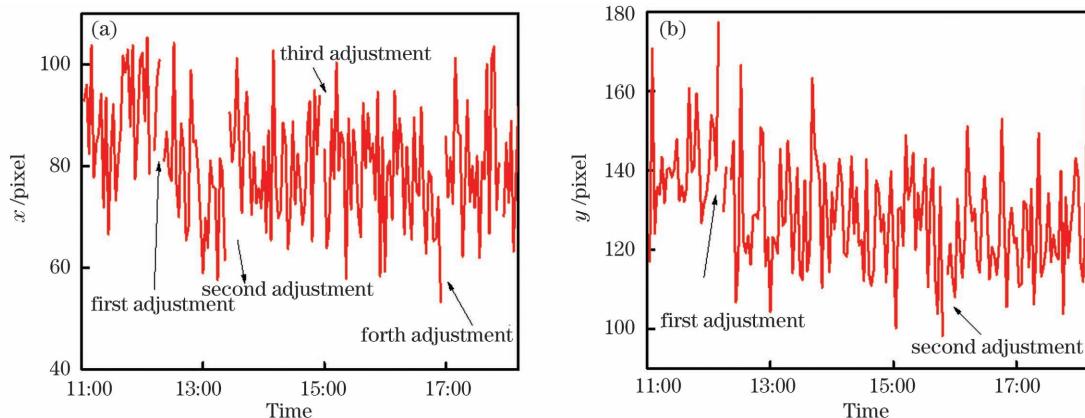
图 13 标定相机探测的 10.3 km 外场实验跟踪曲线。(a)俯仰调整;(b)方位调整

Fig. 13 Tracking curves detected by calibration camera in 10.3 km field experiment. (a) Pitch adjustment; (b) azimuth adjustment

图 14 为 10.3 km 链路无线光通信双向对准实验示意图。激光器 A 发射的光束经大气湍流到达接收端,调整接收端二维反射镜使光束反射至接收马卡天线,经马卡天线和聚焦透镜会聚后,位于接收端的探测器 A 即可探测到发射端的信源信息;激光器 B 的发射光束经过接收天线的焦点位置,由二维反射镜反射后经大气湍流到达发射端,发射端马卡天线和聚焦透镜对光束进行会聚,探测器B可对
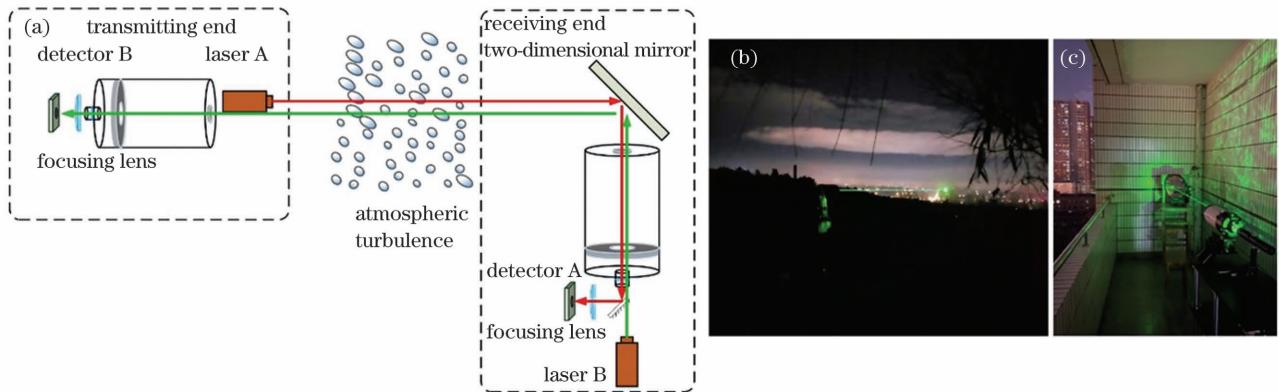
图 14　10.3 km 双向对准实验。(a)系统原理图;(b)发射端;(c)接收端

Fig. 14　Bidirectional alignment schematic in 10.3 km experiment. (a) System schematic; (b) transmitting end;
(c) receiving end

接收端所接收的信源信息进行探测,进而实现光束的双向对准。在调整接收端的二维反射镜过程中,由于光路可逆,在完成发射端到接收端完全对准的同时,即可完成由接收端到发射端的光束对准。图 15 所示为完成双向对准后下行链路探测器输出的波形和上行链路检测的光斑。
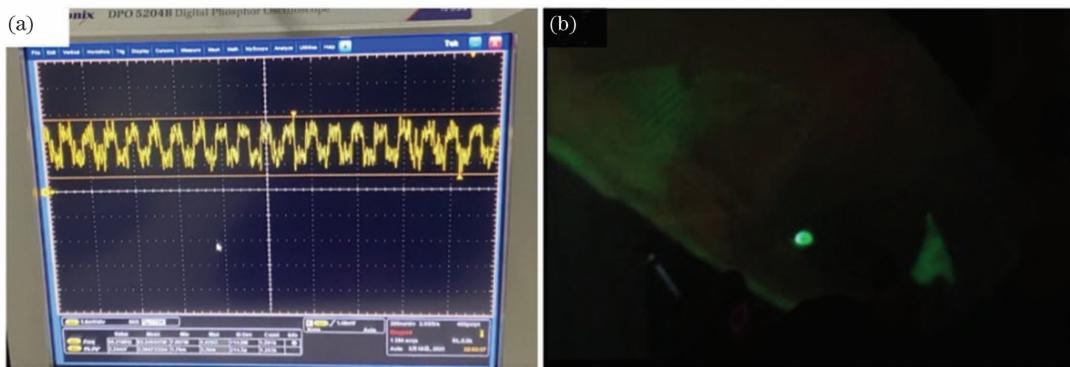
图 15　10.3 km 双向对准实验结果。(a)下行链路传输信号波形;(b)上行链路检测光斑

Fig. 15　Results of 10.3 km bidirectional alignment experiment. (a) Downlink transmission signal waveform; (b) uplink
detection spot

分别计算 10.3 km 通信距离下 x 方向和 y 方向光斑型心变化的均值方差和功率谱密度(图 16),其中 x 方向光斑型心漂移均值为 156.4072 pixel,方差为 18.8653 pixel^2,y 方向光斑型心漂移均值为 118.0435 pixel,方差为 10.5290 pixel^2,x 方向的光斑漂移程度大于 y 方向。随着通信距离的增加,功率谱密度曲线中的低频成分在整体谱密度曲线的占比相比于 1.3 km 实验结果有所减小,大气湍流的
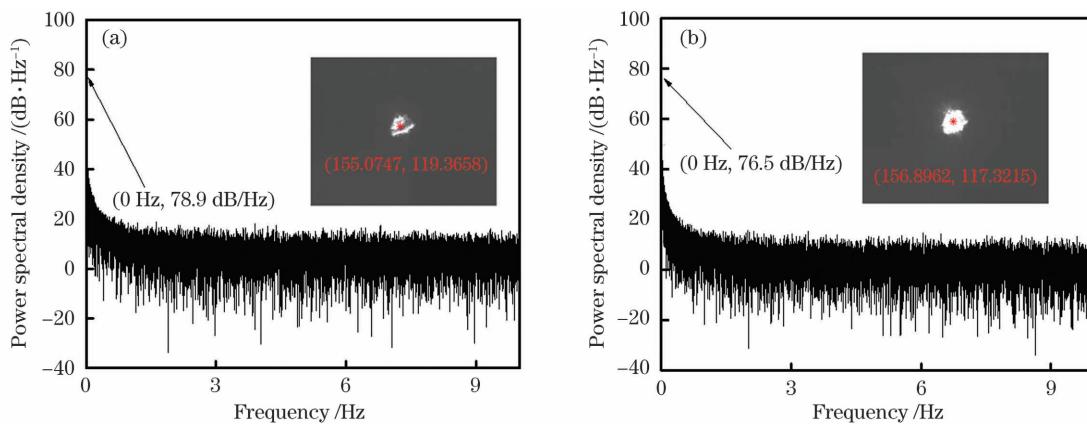
图 16　10.3 km 外场实验中光斑型心漂移量功率谱密度。(a)x 方向;(b)y 方向

Fig. 16　Power spectral density of spot center drift in 10.3 km field experiment. (a) x direction; (b) y direction

增强使得光斑漂移速率明显加快。

图 17 所示为 10.3 km 情形下光束跟踪光斑型心轨迹曲线以及对应的时域波形和功率谱密度,二维反射镜的调整步进角为 10.92 μrad。位于相机中心的光斑型心在 x 方向和 y 方向的方差分别为 14.4970 pixel^2 和 8.0287 pixel^2,其光斑型心调整幅度大于 1.3 km 实验结果,调整轨迹的功率谱密度曲线中低频部分所占的比例也小于 1.3 km 实验结果,这是因为湍流增强所导致的光斑型心漂移量加大,二维反射镜需要调整更大的角度以适应外界环境的变化。

图 18 所示为经跟踪处理后探测器探测得到的波形,其中发射端输出的激光功率为 200 mW,探测器输出波形幅值为 74.4 mV。
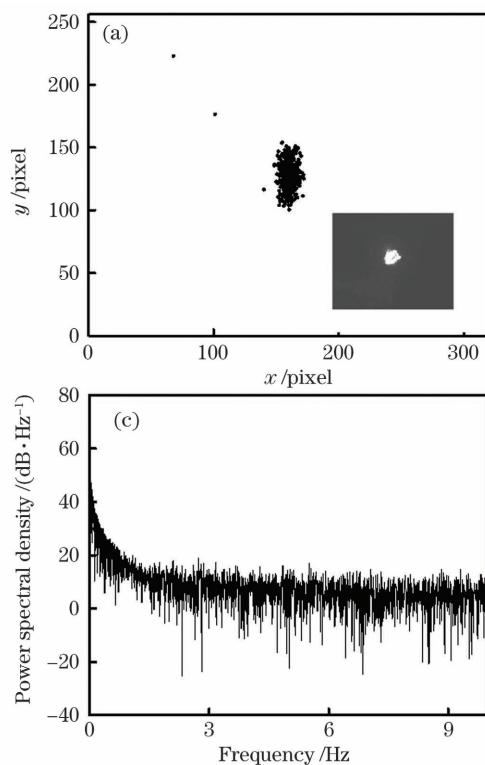
图 17 10.3 km 外场实验的跟踪波形。(a)跟踪轨迹;(b)x、y 方向跟踪曲线;(c)x 方向功率谱密度;(d)y 方向功率谱密度

Fig. 17 Tracking waveforms in 10.3 km field experiment. (a) Tracking curve; (b) track curves along x and y directions; (c) power spectral density along x direction; (d) power spectral density along y direction
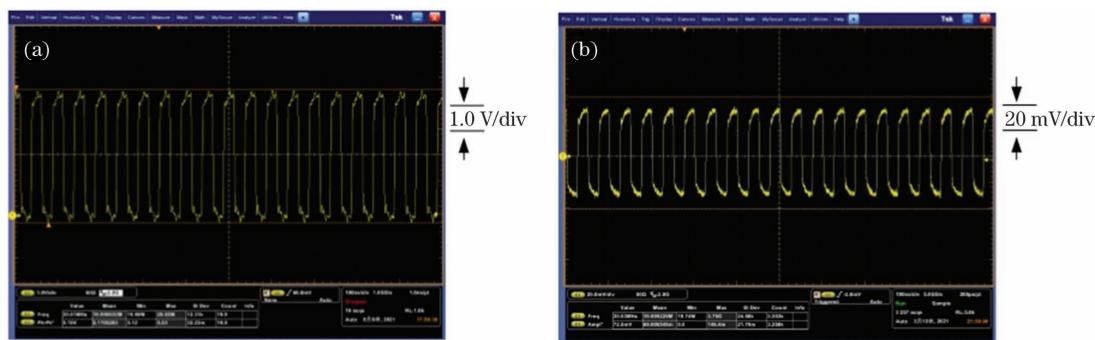
图 18 通信链路 10.3 km 信号波形。(a)发射信号;(b)接收信号
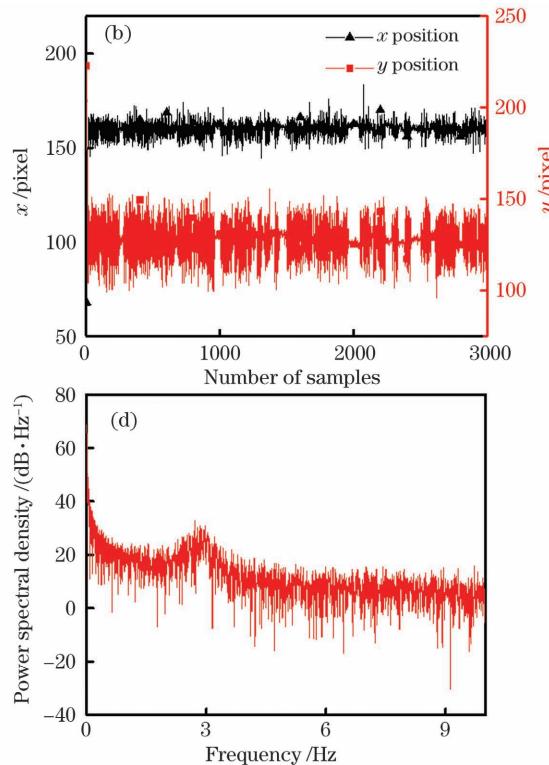
Fig. 18 Signal waveforms at 10.3 km communication link. (a) Transmitting signal; (b) receiving signal

4 结   论

提出一种发射端采用图像标定,接收端采用二维反射镜控制的光束快速对准方法,解决了传统无线光通信中光束对准耗时长的问题。发射端的图像标定粗跟踪可保证光斑有效覆盖二维反射镜,接收端耦合光斑粗跟踪可有效抑制由大气湍流引起的光束漂移,在建立下行链路的同时即可实现上行链路的建立。该方法对大气激光通信光束对准跟踪系统有一定借鉴意义与实用价值。

参 考 文 献

[1] 赵佰秋, 于笑楠, 董岩, 等. 空间激光通信组网反射镜跟踪性能[J]. 激光与光电子学进展, 2021, 58(9): 0906007.
Zhao B Q, Yu X N, Dong Y, et al. Tracking performance of mirrors in space laser communication networking[J]. Laser & Optoelectronics Progress, 2021, 58(9): 0906007.

[2] 孙晶, 黄普明, 幺周石. 大气湍流与平台微振动影响下的星地激光通信性能[J]. 激光与光电子学进展, 2021, 58(3): 0301003.
Sun J, Huang P M, Yao Z S. Performance of satellite-to-ground laser communications under the influence of atmospheric turbulence and platform micro-vibration [J]. Laser & Optoelectronics Progress, 2021, 58(3): 0301003.

[3] Li Q, Liu L, Ma X F, et al. Development of multitarget acquisition, pointing, and tracking system for airborne laser communication[J]. IEEE Transactions on Industrial Informatics, 2019, 15(3): 1720-1729.

[4] Sun X B, Kong M W, Alkhazragi O, et al. Non-line-of-sight methodology for high-speed wireless optical communication in highly turbid water [J]. Optics Communications, 2020, 461: 125264.

[5] Lin J M, Du Z H, Yu C Y, et al. Machine-vision-based acquisition, pointing, and tracking system for underwater wireless optical communications [J]. Chinese Optics Letters, 2021, 19(5): 050604.

[6] Lim H C, Choi C S, Sung K P, et al. Centroid error analysis of beacon tracking under atmospheric turbulence for optical communication links [J]. Remote Sensing, 2021, 13(10): 1931.

[7] 柯熙政, 吴加丽, 杨尚君. 面向无线光通信的大气湍流研究进展与展望[J]. 电波科学学报, 2021, 36(3): 323-339.
Ke X Z, Wu J L, Yang S J. Research progress and prospect of atmospheric turbulence for wireless optical communication[J]. Chinese Journal of Radio Science, 2021, 36(3): 323-339.

[8] Chen M N, Jin X Q, Li S B, et al. Compensation of turbulence-induced wavefront aberration with convolutional neural networks for FSO systems[J]. Chinese Optics Letters, 2021, 19(11): 110601.

[9] 柯熙政, 雷思琛, 杨沛松. 大气激光通信光束同轴对准检测方法[J]. 中国激光, 2016, 43(6): 0606003.
Ke X Z, Lei S C, Yang P S. Beam coaxial alignment detection in atmospheric laser communication [J]. Chinese Journal of Lasers, 2016, 43(6): 0606003.

[10] 柯熙政, 张璞. 一种无线光通信的跟瞄控制系统及跟瞄控制方法: CN110233664A[P]. 2019-09-13.
Ke X Z, Zhang P. A tracking control system and tracking control method for wireless optical communication: CN110233664A[P]. 2019-09-13.

[11] 柯熙政, 卢宁, 赵黎. 一种光束自动捕获装置及光束捕获方法: CN101852924A[P]. 2010-10-06.
Ke X Z, Lu N, Zhao L. An automatic beam capture device and a beam capture method: CN101852924A[P]. 2010-10-06.

[12] Dabiri M T, Sadough S M S, Ansari I S. Tractable optical channel modeling between UAVs[J]. IEEE Transactions on Vehicular Technology, 2019, 68(12): 11543-11550.

[13] Zhang M, Li B, Tong S F. A new composite spiral scanning approach for beaconless spatial acquisition and experimental investigation of robust tracking control for laser communication system with disturbance[J]. IEEE Photonics Journal, 2020, 12(6): 7906212.

[14] 肖永军, 董冉, 熊准, 等. 无线光通信 GPS 辅助定点捕获实验研究[J]. 半导体光电, 2011, 32(6): 833-835, 839.
Xiao Y J, Dong R, Xiong Z, et al. Research on fixed-point acquisition in optical communication based on GPS[J]. Semiconductor Optoelectronics, 2011, 32(6): 833-835, 839.

[15] 肖永军, 艾勇, 董冉, 等. 基于 ATP 系统的非机动目标跟踪实验[J]. 红外与激光工程, 2012, 41(9): 2439-2443.
Xiao Y J, Ai Y, Dong R, et al. Experiment of non-maneuvering target tracking based on ATP system [J]. Infrared and Laser Engineering, 2012, 41(9): 2439-2443.

[16] 谭立英, 吴世臣, 韩琦琦, 等. 潜望镜式卫星光通信终端的 CCD 粗跟踪[J]. 光学 精密工程, 2012, 20(2): 270-276.
Tan L Y, Wu S C, Han Q Q, et al. Coarse tracking of periscope-type satellite optical communication terminals [J]. Optics and Precision Engineering, 2012, 20(2): 270-276.

[17] 柯熙政, 王姣. 一种基于四象限探测器的光斑对准方法: CN106767543B[P]. 2019-11-22.
Ke X Z, Wang J. A spot alignment method based on four quadrant detector: CN106767543B[P]. 2019-11-22.

[18] 陈少杰, 张亮, 王建宇. 数模转换器分辨率对捕获、跟踪、瞄准系统跟踪精度的影响[J]. 中国激光, 2017, 44(8): 0806004.
Chen S J, Zhang L, Wang J Y. Effects of digital to analog converter resolution on ATP system tracking accuracy[J]. Chinese Journal of Lasers, 2017, 44

(8)：0806004．

[19] Chen M W, Yang Y P, Jia X T, et al. Investigation of positioning algorithm and method for increasing the linear measurement range for four-quadrant detector[J]. Optik, 2013, 124(24): 6806-6809.

[20] 刘云清，姜会林，佟首峰．大气激光通信中稳定跟踪器件及算法研究[J]．中国激光，2011，38（5）：0505005．
Liu Y Q, Jiang H L, Tong S F. Study on stabilizational tracking technology for atmospheric laser communication system[J]. Chinese Journal of Lasers, 2011, 38(5): 0505005.

[21] 李生民，张圆清．空间激光通信中四象限光电探测器环形光斑检测及误差补偿[J]．中国激光，2017，44（11）：1106005．
Li S M, Zhang Y Q. Annular facula detection and error compensation of four-quadrant photoelectric detector in space laser communication[J]. Chinese Journal of Lasers, 2017, 44(11): 1106005.

[22] Vo Q S, Zhang X D, Fang F Z. Extended the linear measurement range of four-quadrant detector by using modified polynomial fitting algorithm in micro-displacement measuring system[J]. Optics & Laser Technology, 2019, 112: 332-338.

[23] Bao J Y, Xing F, Sun T, et al. CMOS imager non-uniformity response correction-based high-accuracy spot target localization[J]. Applied Optics, 2019, 58 (16): 4560-4568.

[24] Zhang W G, Guo W, Zhang C W, et al. An improved method for spot position detection of a laser tracking and positioning system based on a four-quadrant detector[J]. Sensors, 2019, 19(21): 4722.

[25] 陈刚，董作人，耿健新，等．155/622 Mb/s 多发射器激光通信系统[J]．中国激光，2004，31（5）：583-587．
Chen G, Dong Z R, Geng J X, et al. 155/622 Mb/s multiple transmitter laser communication systems[J]. Chinese Journal of Lasers, 2004, 31(5): 583-587.

[26] Tolker-Nielsen T, Oppenhauser G. In-orbit test result of an operational optical intersatellite link between ARTEMIS and SPOT4, SILEX [J]. Proceedings of SPIE, 2002, 4635: 97-104.

[27] Liu W, Yao K N, Huang D N, et al. Performance evaluation of coherent free space optical communications with a double-stage fast-steering-mirror adaptive optics system depending on the Greenwood frequency[J]. Optics Express, 2016, 24 (12): 13288-13302.

[28] Chang Q B, Chen W S, Liu J K, et al. Development of a novel two-DOF piezo-driven fast steering mirror with high stiffness and good decoupling characteristic [J]. Mechanical Systems and Signal Processing, 2021, 159: 107851.

[29] Dubra A, Massa J S, Paterson C. Preisach classical and nonlinear modeling of hysteresis in piezoceramic deformable mirrors[J]. Optics Express, 2005, 13 (22): 9062-9070.

[30] 左韬，黄海波，肖永军．基于自校正控制的空间光通信精跟踪系统设计[J]．仪器仪表学报，2012，33（5）：1181-1186．
Zuo T, Huang H B, Xiao Y J. Fine tracking system design of space optical communication based on self-tuning control [J]. Chinese Journal of Scientific Instrument, 2012, 33(5): 1181-1186.

[31] Jono T, Toyoshima M, Takahashi N, et al. Laser tracking test under satellite microvibrational disturbances by OICETS ATP system [J]. Proceedings of SPIE, 2002, 4714: 97-104.

[32] Borrello M. A multi stage pointing acquisition and tracking (PAT) control system approach for air to air laser communications[C]//Proceedings of the 2005, American Control Conference, 2005, June 8-10, 2005, Portland, OR, USA. New York: IEEE Press, 2005: 3975-3980.

[33] Suite M R, Burris H R, Moore C I, et al. Fast steering mirror implementation for reduction of focal-spot wander in a long-distance free-space optical communication link[J]. Proceedings of SPIE, 2004, 5160: 439-446.

[34] 王福超，王昱棠，田大鹏．音圈快速反射镜的完全跟踪控制[J]．光学 精密工程，2020，28（9）：1997-2006．
Wang F C, Wang Y T, Tian D P. Perfect tracking control for fast-steering mirror driven by voice coil motor[J]. Optics and Precision Engineering, 2020, 28(9): 1997-2006.

[35] Wu X, Chen S H, Shi B Y, et al. High-powered voice coil actuator for fast steering mirror[J]. Optical Engineering, 2011, 50(2): 023002.

[36] 陈国真，徐斯强，刘品宽，等．大行程快速反射镜的结构设计及带宽特性[J]．光学 精密工程，2020，28（1）：90-101．
Chen G Z, Xu S Q, Liu P K, et al. Structural design and bandwidth characteristic of a fast steering mirror with large travel range [J]. Optics and Precision Engineering, 2020, 28(1): 90-101.

[37] Pokorny P. One-mirror and two-mirror three-dimensional optical scanners: position and accuracy of laser beam spot[J]. Applied Optics, 2014, 53(12): 2730-2740.

Fast Alignment of Wireless Optical Communication Using Two-Dimensional Mirror

Yang Shangjun[1], Ke Xizheng[1,2,3*], Wu Jiali[1], Liu Xuguang[4]

[1] *School of Automation and Information Engineering, Xi'an University of Technology, Xi'an 710048, Shaanxi, China;*

[2] *Shaanxi Civil-Military Integration Key Laboratory of Intelligence Collaborative Networks, Xi'an 710048, Shaanxi, China;*

[3] *School of Physics and Telecommunications Engineering, Shaanxi University of Technology, Hanzhong 723001, Shaanxi, China;*

[4] *Department of Communication Engineering, School of Automation and Information Engineering, Xi'an University of Technology, Xi'an 710048, Shaanxi, China*

Abstract

Objective   When the laser signal is transmitted through the atmospheric channel, the fluctuation of atmospheric refractive index caused by atmospheric turbulence causes beam expansion, beam drift, and wavefront distortion, which harms the reception of the optical signal and even leads to the interruption of communication in severe cases. In a wireless optical communication system, the gaze-gaze, gaze-scan, and skip-scan are used to achieve the coaxial alignment of the beam between the transmitting and receiving antennas, which increases the preparation time of system communication. In practice, a fast acquisition, tracking, and alignment mechanism must establish links.

The wireless optical communication system's coaxial alignment demands that the optical axis of the transmitting and receiving antennas completely coincide in space. The detector must return the measured parameter data to adjust the transmitting antenna to keep the beam stable coarse alignment for a long time and fine alignment on this basis. Atmospheric turbulence affects long-distance data return and position adjustment, making the traditional long-axis beam alignment process uncertain.

In this paper, an acquisition tracking and pointing system with independent transceiver control is developed. The transmitter calibrates and tracks the target position by the calibration camera to realize the course alignment of the beam; at the receiving end, a two-dimensional mirror is used to control the position as the spot center feedback, suppress the atmospheric turbulence, and realize the fine alignment of the beam. The non-common sight axis control avoids the inconvenience of transmitting control instructions from the receiving end to the transmitting end, and it is not necessary to use a space stable platform for the moving base, which greatly facilitates the promotion of wireless optical communication.

Methods   Fig. 1(b) shows the wireless optical communication using a two-dimensional mirror-assisted alignment. The system comprises the calibration coarse alignment from the transmitting antenna to the two-dimensional mirror and the minor axis fine alignment from the two-dimensional mirror to the receiving antenna. The coarse alignment from the transmitting antenna to the two-dimensional mirror is directly positioned and calibrated by the calibration camera at the transmitting end, and the transmitting antenna is adjusted with the image as feedback; fine alignment from the two-dimensional mirror to the receiving antenna is adjusted by the two-dimensional mirror based on the detector feedback information at the back end of the receiving antenna. As the calibration coarse alignment and minor axis fine alignment can be operated at a single end, the calibration alignment at the transmitting end does not require data return.

Fig. 4 depicts the construction of a wireless optical communication IM/DD system that uses a two-dimensional mirror to achieve rapid alignment. The transmitting end loads the source by intensity modulation, and the output is collimated by the transmitting antenna. To complete the initial calibration, the aiming platform at the transmitting end and the calibration camera connect with the two-dimensional mirror at the receiving end, so that the beam completely covers the two-dimensional mirror at the receiving end, thus, adjusting the two-dimensional mirror to align the reflected beam coaxial with the receiving antenna. The parallel light emitted by the receiving antenna passes through the optical prism is divided into two beams. The focusing lens converges to one of the beams, which is coupled into the photosensitive surface of the photodetector for system communication; the other beam is focused, and the infrared camera detects the spot position in real-time to complete the beam tracking.

Results and Discussions   After course alignment, the beam is tracked based on the relative deviation between the calibration point and the imaging coordinate position of the two-dimensional mirror. Fig. 7 shows the beam course tracking curve of the position coordinate of the two-dimensional mirror under the 1.3 km experimental link, in which the pitch and azimuth angles are adjusted twice and once in four hours, respectively. The beam drift is caused by atmospheric turbulence; the gravity subsidence and mechanical vibration of the optical-mechanical structure makes frequently adjusting the coarse alignment in a short time unnecessary.

Fig. 10 shows the 1.3 km beam-tracking curve, the corresponding time-domain waveform, and power spectral density estimation. The step angle of the two-dimensional mirror is adjusted to 10.92 μrad. With the increase of the iteration numbers, the center of the spot is gradually adjusted from the first quadrant of the detection surface to the center. After tracking, the variations of the spot centroid at the center of the camera in the x and y directions are 2.2770 and 1.3697 pixels^2, respectively. The time required to perform one closed loop is 0.05 s, which is sufficient to compensate for the drift rate of the spot.

Fig. 14 shows the bidirectional alignment experiment for a 10.3 km wireless optical communication link. After the beam emitted by the laser reaches the receiving end through atmospheric turbulence, the two-dimensional mirror at the receiving end is adjusted to reflect the beam to the receiving antenna. The detector at the receiving end can detect the source information from the transmitting end after converging by an antenna and focusing lens. Laser B emits a light beam at the focus position of the receiving antenna, which is reflected by the two-dimensional mirror and reaches the transmitting end through atmospheric turbulence. To achieve the two-way alignment of the light beam, the antenna and the focusing lens at the transmitting end converge the light beam, and detector B can detect the source information transmitted by the receiving end. By adjusting the two-dimensional mirror at the receiving end, the beam alignment from the receiving to the transmitting end can be accomplished while completing the entire alignment from the transmitting to the receiving end because the optical path is reversible.

Conclusions   This study presents a method for achieving rapid beam alignment using image calibration at the transmitting end and a two-dimensional mirror control at the receiving end, thus, addressing the problem of long time-consuming beam alignment in traditional wireless optical communication. The image calibration coarse tracking at the transmitting end can ensure that the spot effectively covers the two-dimensional mirror, and the coupling spot coarse tracking at the receiving end can effectively suppress the beam drift caused by atmospheric turbulence; the uplink can be established simultaneously with the downlink. The non-common sight axis control avoids the inconvenience of transmitting control instructions from the receiving end to the transmitting end, and it is not necessary to use a space stable platform for the moving base, which greatly facilitates the promotion of wireless optical communication.

Key words   optical communications; beam scanning; acquisition tracking alignment; two-dimensional mirror